Magnesium Technology 2012
Edited by: Suveen N. Mathaudhu, Wim H. Sillekens, Neale R. Neelameggham, and Norbert Hort
TMS (The Minerals, Metals & Materials Society), 2012

SOLID STATE JOINING OF MAGNESIUM TO STEEL

Saumyadeep Jana[1], *Yuri Hovanski*[1], Siva P Pilli[1], David P Field[2], Hao Yu[2], Tsung-Yu Pan[3], M L Santella[3]
[1]Pacific Northwest National laboratory, Richland, WA, 99354, USA
[2]Washington State University, Pullman, WA, 99164-2920, USA
[3]Oak Ridge National Laboratory, Oak Ridge, TN 37381-6096, USA

Keywords: Magnesium, Steel, Friction stir welding, Ultrasonic welding

Abstract

Friction stir welding and ultrasonic welding techniques were applied to join automotive magnesium alloys to steel sheet. The effect of tooling and process parameters on the post-weld microstructure, texture and mechanical properties was investigated. Static and dynamic loading were utilized to investigate the joint strength of both cast and wrought magnesium alloys including their susceptibility and degradation under corrosive media. The conditions required to produce joint strengths in excess of 75% of the base metal strength were determined, and the effects of surface coatings, tooling and weld parameters on weld properties are presented.

Introduction

The U.S. Department of Energy's (DOE) Vehicle Technologies Program (VTP) is leading the development of high-performance, cost-effective materials-and the processes needed to manufacture them-to make advanced vehicles more fuel efficient and affordable. One key goal is to validate a cost-effective 50% weight reduction in passenger-vehicle body and chassis system by 2015 [1]. Recently, a joint project between VTP and U.S. automakers overcame several hurdles to the introduction of lightweight magnesium components, resulting in a magnesium engine cradle for the Chevy Corvette Z06 that is nearly 60% lighter than a steel cradle [1]. A key combination of low density, and high specific strength makes magnesium alloys an ideal choice for automotive applications because of the associated effect of weight reduction on better fuel economy. Though currently there are no adequate wrought magnesium alloys available to meet the requirements of automotive body applications, extensive research is taking place to enhance the properties of magnesium sheet products [2]. Steel, on the other hand, is currently the automaker's material of choice. This is because cold rolled mild steel offers excellent ductility, consistent properties and low overall component production costs. However, in a modern multi-material vehicle, lightweight materials such as aluminum and magnesium alloys can be a challenge to join and attach to the underlying sub-structure, usually composed of steel. Joining methodologies available in the cost environment relevant to automotive manufacturing include resistance spot welding, adhesives, linear fusion welding, hemming, clinching, bolting, and riveting [3].

However, joining Magnesium to steel poses a specific challenge. The maximum solid solubility of Fe in (Mg) is 0.00043 at%, and solid solubility of Mg in (Fe) is nil [3]. Melting points of Mg and Fe are 922 K (649 °C) and 1812 K (1539 °C), respectively. This huge difference in melting points makes it very difficult to melt both metals at the same time as might be required for fusion welding processes. Moreover, both metals are immiscible in a liquid state, and they do not react to form any congruent melting phase(s). Therefore, joining Mg alloys to steels through conventional fusion welding is problematic at best. Recently, laser-GTA hybrid welding technique was tried to join AZ31B alloy to 304 steel in lap configuration with AZ31B on top [4]. Results indicate poor joining strength and Mg-Fe interfacial fracture. The authors attributed such low mechanical strength to severe oxidation at Mg/Fe interface. Joining methods that require a large amount of plastic strain in the magnesium component suffer from magnesium's poor ductility at room temperature.

A recent DOE funded project looked at the feasibility of joining magnesium to steel through solid state route. Two specific joining technologies, e.g., friction stir welding and ultrasonic welding, were examined in this program. Pacific Northwest National Laboratory (PNNL) played the lead role in developing the friction stir welding route. A few recent studies indicate that friction stir welding (FSW) has the ability to join Mg alloys to steel [5,6]. FSW, which is a solid state welding technique invented by Thomas et al. at TWI, UK [7], has the added advantage of minimal associated oxidation because of the solid state nature of the process. A short preliminary effort at PNNL indicated higher joint strength in Mg to steel lap welds when the bottom steel sheet was deformed by the FSW tool [8].

Ultrasonic welding (USW) of Mg alloys to steel sheet was developed at the Oak Ridge National Laboratory (ORNL). The work focused on identifying the factors critical to increasing joint strength while understanding the influence of sonotrode tip design, material stack-up, coatings, and process time.

Summary of the FSW Initiative

Following our initial trial, an effort was made to optimize the FSW tool design in order to increase the Mg/steel joint strength in lap configurations. Two tool designs were tested in this study. The first tool (Tool 1) had a convex scrolled shoulder and a stepped spiral pin. The second tool (Tool 2) had identical features as the first tool plus a short hard WC insert on the tool pin bottom. Both the tools were made of H13 tool steel. A nominally 2.32 mm thick AZ31 magnesium alloy (O temper) was used as the top sheet. Two different steels were used, e.g., (i) HDG 1.5 mm thick HSLA steel and (ii) EG 0.8 mm thick mild steel (MS), as the bottom sheet material. Mechanical performance of the joints was determined through quasi-static unguided lap-shear tests, and fatigue tests. Further, joint interface microstructure was characterized in detail using optical microscope/SEM. Additionally, EBSD technique was employed to learn about the crystallographic information at the joint interface.

The welding was carried out in position controlled mode in a high stiffness, precision FSW machine manufactured by TTI, Inc. and located at PNNL. Complete details about the welding procedure has been published elsewhere [3,8]. Subsequently, three to five lap-shear specimens of width ~30 mm were obtained for each weld covering the entire weld length. Tensile tests were carried out at room temperature at a crosshead speed of 1 mm/min. Both ends of the lap-shear specimens were appropriately

shimmed in order to minimize misalignment. Average failure load of a standard 30 mm wide lap-shear AZ31/MS weld coupon varied between 4.6 to 6.8 kN, as a function of process parameters. In the case of AZ31/HSLA weld coupons, the average failure load varied between 3.7 to 9.7 kN. Comparison of the lap-shear data revealed that the failure load was generally higher in the case of AZ31/HSLA welds, reflecting the higher strength of the bottom steel sheet used therein. Moreover, use of Tool 2 helped in lowering the scatter.

For graphical comparison purpose, weld efficiency of all the joints were calculated by comparing the failure load of the joint, with the maximum load carrying capacity of the weaker parent sheet section. Whichever parent sheet section shows a lower total load carrying capacity, is noted to be the weaker one. 0.8 mm steel is the weaker one for AZ31/MS welds, and AZ31 sheet is the weaker one for AZ31/HSLA welds. For calculating joint efficiency, the following equation was used:

$$\text{Joint efficiency} = (\text{Max. load of joint} / (A_w \times TS_{\text{parent sheet}})) \times 100$$

A_w is the area of the weaker parent sheet section, and TS is the tensile strength. Weld efficiency data for all the welds are shown in Figure 1a and 1b. The average minimum joint efficiency is

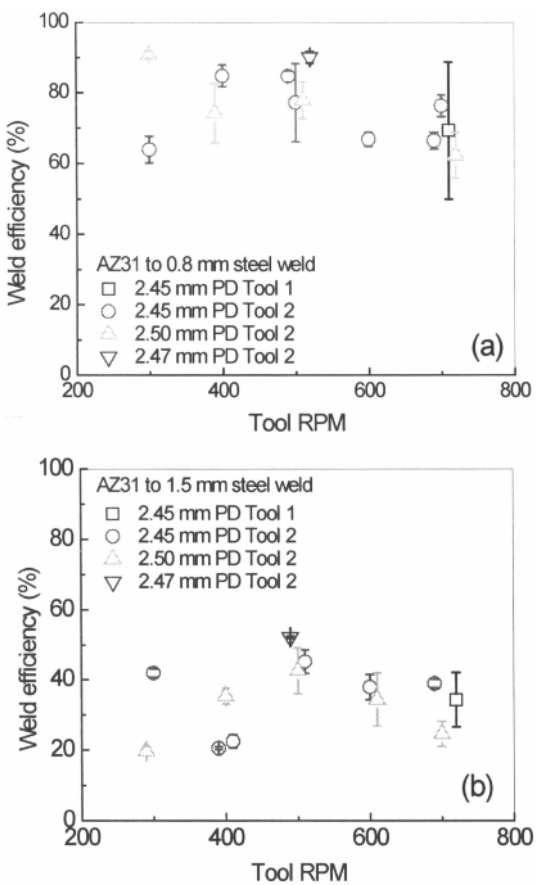

Figure 1. Weld efficiency plots: (a) AZ31/MS, (b) AZ31/HSLA.

>60 % in the case of AZ31/MS welds, and ~40% for AZ31/HSLA welds. Joint efficiency varied as a function of process parameters. Further, the benefit of using Tool 2 in order to obtain uniform strength is evident from the weld efficiency plots. Maximum joint efficiency is achieved at ~500 tool RPM for the AZ31/MS welds, with a tool plunge depth of 2.45 mm (Fig. 1a). For AZ31/HSLA welds, the highest joint efficiency is noted at 500 tool rotation rate, with the tool plunge depth being 2.50 mm (Fig. 1b). Based on the lap-shear test data, a single tool rotation rate of 500 rpm at an intermediate tool plunge depth of 2.47 mm was selected to carry out further welds. It should be noted that the tool travel speed was fixed at 100 mm/min for the entire study. The combination of 500 RPM, 100 mm/min travel speed, and 2.47 mm plunge depth resulted in >90% weld efficiency in the case of AZ31/MS welds. At same process parameters, weld efficiency of AZ31/HSLA weld was noted to ~52%, which was the highest in its class. Additionally, one of the AZ31/MS weld specimens at this particular combination of process parameters showed failure of the steel sheet, leaving the weld intact. The example of such a lap-shear specimen is shown in Figure 2.

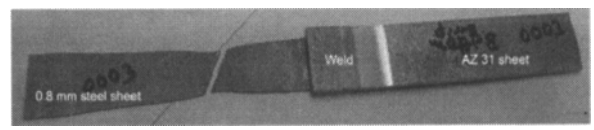

Figure 2. A lap-shear specimen: failure occurred by steel sheet fracture, leaving the weld intact.

Following quasi-static testing, performance of the lap joints at the best process parameters was determined under dynamic loading. A number of 30 mm wide lap-shear weld coupons were tested in a servo-hydraulic fatigue testing machine at a load ratio R of 0.1. The test frequency was 5 Hz. Fatigue tests were conducted in the load-control mode. S-N plot of the lap-shear fatigue specimens is represented in Fig. 3. At similar fatigue lives, the maximum

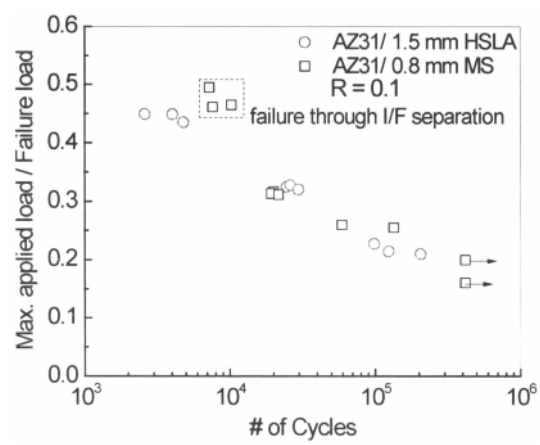

Figure 3. S-N plot for the Mg/steel friction stir lap welded specimens.

applied loads are found to be higher for the AZ31/HSLA welds than the AZ31/MS welds, reflecting the higher failure load of the AZ31/HSLA welds. However, when the maximum applied load is normalized against the respective failure load, as shown in Fig. 4, specimens from both material combinations are noted to have similar fatigue lives at any given applied load to failure load ratio. The major mode of failure was found to be top Mg sheet fracture.

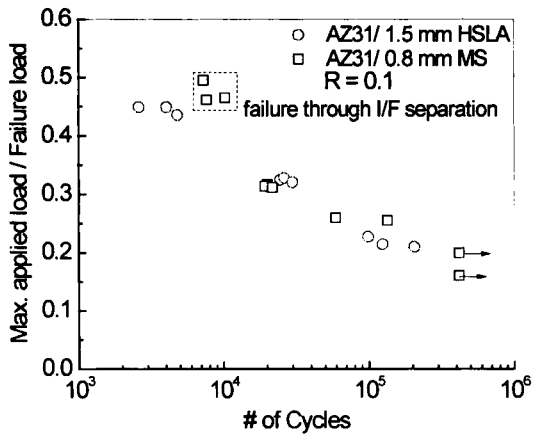

Figure 4. Normalized S-N plot for the Mg/steel friction stir lap welded specimens.

However, three AZ31/MS weld specimens that were tested at 3 kN, showed relatively longer life. Interfacial separation of the top and bottom sheet was the mode of failure for these three specimens. It can be further noted from Fig. 4 that two of the AZ31/MS weld specimens did not fail when applied load to failure load ratio was less than 0.2. Fatigue tests for these two specimens were stopped at ~$5x10^5$ cycles.

A typical cross-section image of a joint fabricated by Tool 2 is shown in Figure 5a. The effect of the WC insert on the tool pin bottom is clearly evident on this image. Presence of the insert resulted in machining of the bottom steel sheet. Further, it led to the formation of two "dove-tail" like features on both ends, as noted by the arrows. Some of the higher magnification SEM images obtained from various locations along the joint interface are shown in Figure 5b and 5c. Microstructural features observed in these images, indicate formation of solidification products through eutectic reaction, due to the melting of the Zn coating present on the steel sheet. However, no such solidification product was found along the region where the steel sheet showed signs of deformation due to the penetrating action of the tool. As the FSW tool plunges through the top Mg sheet, the Zn coating on the bottom steel sheet melts. The liquid Zn layer dissolves Mg from the top Mg sheet, and, hence forms a liquid Zn-Mg alloy. However, this newly formed liquid alloy layer gets squeezed out laterally due to the forging action of the tool.

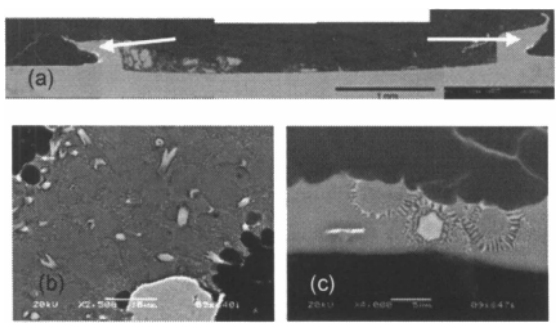

Figure 5. (a) Cross-section of a joint fabricated by Tool 2, (b),(c) Eutectic microstructure at Mg/steel interface.

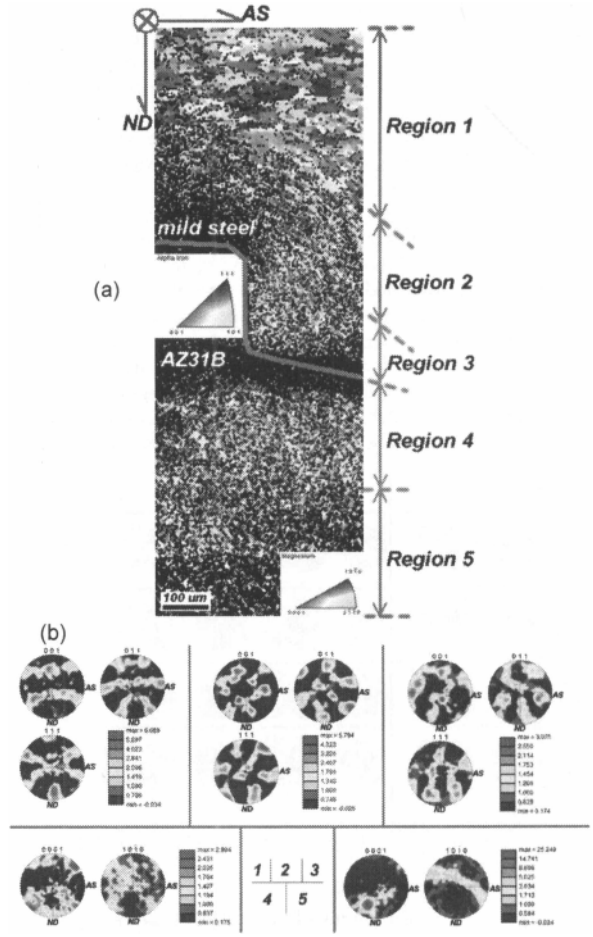

Figure 6. (a) Orientation map of the interface region at the advancing hook of FSW of AZ31B to mild steel, (b) Pole figures of the different regions in shown in (a).

A detailed EBSD study was carried out to characterize the weld nugget and the Mg/steel interface. As shown in Fig 6a, the area around the advancing hook in the FSW of AZ31B to mild steel could be divided into five regions. Region 1 is the base metal of the mild steel and there is no influence of the shear that happens in this region. Region 2 is the region near the interface which lies between the hook area and the base metal. The grains in this region are elongated in the shear direction. Due to the influence of the shear, the grains' thickness decreases as shear increases. Several shear textures form in this region. Region 3 is the region of hook near the weld nugget. The strain is heavy in this region. Grains in this region show a different orientation to the other region of the steel. Region 4 is the interface region of the Mg side. The texture differs to that of the steel side. Region 5 is the region near the weld nugget. The pole figures of each region are shown in Fig.6b.

Fig.6b-1 shows the texture of the base metal of the mild steel. The maximum intensity of the pole figure is 8.069. Fig.6b-2 shows the texture of the interface region of the steel side. The grains in that region rotated in favor of the shear and the strength of the texture decreased to 5.794. The texture of the interface near the weld nugget was influenced by the lower surface of the pin

and the side face of the tip. The texture is randomized in this region and the maximum intensity decreases to 3.075. The interface of the Mg side shows a texture much like that of normal direction (ND)-advancing side. The two components of the texture are perpendicular to each other. The maximum strength of the texture is only about 2.904. The texture of the Mg side away from the interface shows a strong texture. The maximum intensity of the pole figures of that region is 25.249.

The pole figures of the weld nugget region are shown in Fig. 7. The texture changes little in the ND in the region far away from the shoulder and the interface. The rotation of shoulder and the pin forms a truncated cone and the crystals within the cone have their basal planes parallel to the cone surface. The direction of the crystalline alignment is due to the local change of the shear direction. The texture under the shoulder is influenced by the lower surface of the shoulder, and the texture changes little in this nugget region. The texture near the interface differs from that of the weld nugget, but the texture strength in this region is low.

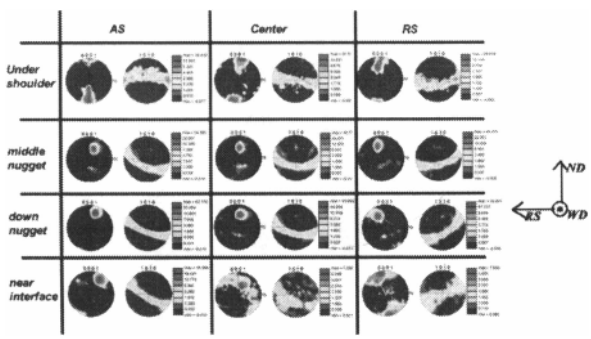

Figure 7. Pole figures of the nugget region of FSW of AZ31B to HSLA

Summary of the USW Initiative

The ultrasonic welds for this study were made with a Sonobond CLF2500 pedestal welding station. The rated conditions at the welding tip were 20 kHz frequency with 25 micrometers (μm) amplitude. The sonotrode tips were made from T1 steel. They typically have flat, rectangular faces with dimensions of either 5 mm x 7 mm or 7 mm x 7 mm. The line pressure to the tip clamping mechanism was adjusted to make the welds under constant nominal pressure of 39 MPa.

The materials used for the current experiments were sheets of 0.8-mm-thick hot-dip-galvanized (HDG) mild steel and 1.6-mm-thick AZ31B-H24. The zinc coating on the steel was about a 9 μm-thick. Prior to welding the surfaces of the AZ31B sheet were buffed with non-metallic abrasive pads to remove surface oxides and produce shiny surfaces. Both metals were also degreased with acetone followed by isopropyl alcohol to remove lubricants and surface debris.

Coupons of AZ31 nominally 30 mm wide x 100 mm long were welded to mild steel coupons of the same size to produce specimens for mechanical testing and metallographic analysis. A 25 mm overlap was used for making lap-welded coupons with spot welds centered in the overlap regions. Specimens were positioned for welding so that the primary vibration direction of the sonotrode was perpendicular to their long axis. Spot welding was typically performed using power of 1500-2500 W, and welding times ranged from 0.2-1.2 s.

The results of the tensile lap-shear testing are presented in Figure 8 where the variations of failure load with welding time are plotted. With both tips there was an initial rapid rise in lap-shear failure load from around 0.5 kN to near 2.9 kN as the welding times increased from 0.2-0.4 s. After the noted increase, failure loads continued increasing with welding times but at a much lower rate. From 0.4-1.2 s, failure loads increased to a maximum average value of 3.7 kN for the 5-mm x 7-mm tip and 4.2 kN for the 7-mm x 7-mm tip. Welds of the AZ31 to bare steel were unsuccessful. Weak bonding occurred in this case, but joints could be easily broken by hand.

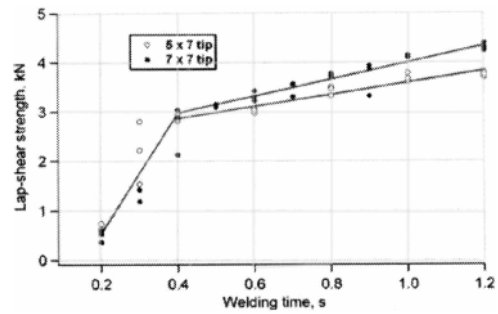

Figure 8. Variations of lap-shear strength with welding time and tip size

The lap-shear strength results can be placed in perspective by comparison with data from resistance spot welds and friction stir spot welds of AZ31. Published work [9] confirmed that AZ31 could be resistance spot welded with lap-shear strengths ranging to 5.7 kN. Lap-shear strengths increased with spot diameters and were about 4.0 kN for diameters with areas equivalent to the 7-mm x 7-mm USW tip. More recently, Lang and co-workers [10] measured lap-shear strengths up to 3 kN for spot welds of AZ31 with nugget diameters of about 7 mm. Another published study showed that AZ31 sheet could be friction stir welded and some joints had lap-shear strengths as high as 4.75 kN. No comparable published data could be found for magnesium-steel spot-welded joints made by these two processes. Nevertheless, strengths for ultrasonically-welded joints at times greater that about 0.5 s consistently exceeded 3 kN and so they are generally consistent with values found for magnesium-magnesium spot welds.

The results of the fatigue testing are shown as Figure 9 where the fatigue life expressed as cycles to failure is plotted against the load range for testing. The USW spot welds were tested at constant values of R = 0.1 and R = 0.2, where R = minimum load/maximum load.

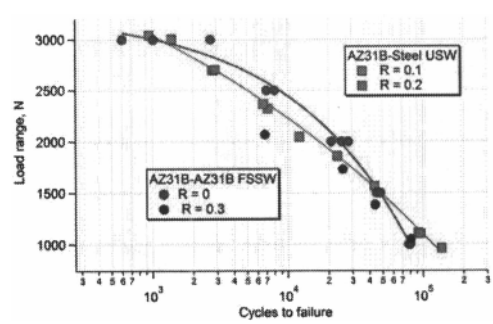

Figure 9. Variations of fatigue life expressed as cycles to failure with loading range

There are few published data for similar or dissimilar spot welds involving magnesium alloys, and Figure 9 compares the USW data to similar data from friction stir spot welds of AZ31-to-AZ31 lap welds. Regression analysis was used for the lines drawn through the USW data at R = 0.1 and the FSSW data of R = 0.0. However, a single line could have been fit through the entire combined data set. This suggests the fatigue properties of the AZ31-steel USW spots welds will not differ significantly from other types of spot welds made using AZ31. A more detailed examination of the fatigue performance for this work was previously documented [11, 12].

Additional results from tensile lap-shear testing are presented in Figure 10 where the variations of failure load with welding time are plotted for two arrangements: Mg-steel, where the sonotrode engaged the AZ31, and Steel-Mg, where the same engaged the hot-dip- galvanized (HDG) steel. The maximum lap-shear failure loads for Mg-steel spot welds are near 4 kN for 1.0 s of welding time. Those lap-shear strengths are in the range of the levels found for resistance spot welding and friction stir spot welding AZ31 to itself [9,10]. Given the disparities of properties between AZ31 and the mild steel, the lap-shear results are remarkable. Figure 10 indicates that similar maximum failure loads can be achieved with the either arrangement. This important result indicates that the USW has desirable flexibility in how it is presented to components in the manufacturing environment.

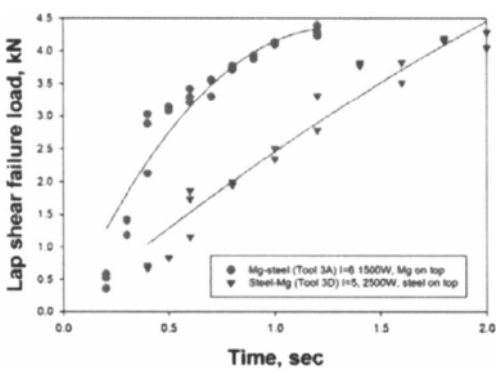

Figure 10. Variations of lap-shear strength with welding time and metal arrangement using a 7-mm x 7-mm sonotrode tip

One additional point of interest was the evaluation of hybid joining. Initial results from this evaluation are presented in Figure 11 where the Mg-steel results are replotted for comparison. Results are shown for three adhesive (Dow Betamate 73305) situations. First, USW spot welds were made through uncured adhesive as is commonly done with resistance spot welding. This approach caused a significant decrease of lap-shear strength. Subsequently, some spot welded coupons were cured. Curing produced lap-shear strengths in the range of 6 kN. As a reference, coupons that were only adhesive bonded and cured were also tested, and these had lap-shear strength of 4-5 kN. These results suggest that USW spot welding through adhesive is not advisable. Presumably, this is at least partial due to the adhesive modifying friction properties at the welded interface. Additional studies will be required to determine how much strength can be preserved in USW spot welds made through uncured adhesives. Once the adhesive is cured, lap-shear strengths can exceed those made by either processes alone. In all of the experiments, the area covered by adhesive was approximately 25 mm x 25 mm, a significantly larger area than that of the USW spot welds, approximately 7 mm x 7 mm.

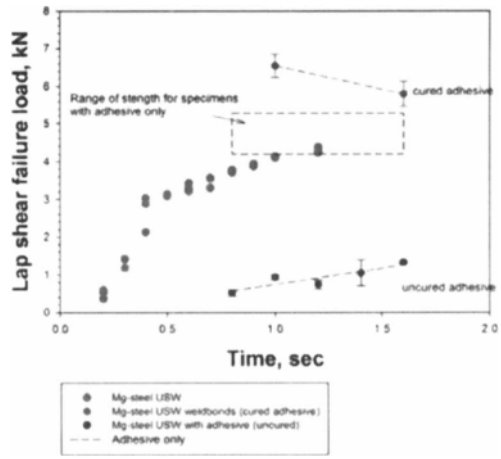

Figure 11. Variations of lap-shear strength with welding time and adhesive cure condition

Finally, results from an evaluation of the effect of corrosion on lap-shear strength are shown in Figure 12. A total of 20 Mg-steel specimens were made for exposure using the Ford Arizona Proving Ground Equivalent Corrosion Cycle (APGE) test, a widely accepted screening test for automotive industry. The exposure consisted of immersion in 5% NaCl bath at room temperature for 15 minutes followed by air-drying for 3 hours. Following this, the dried specimens were placed in a chamber where relative humidity was controlled to 80% and temperature was maintained at 50°C. Each cycle of exposure in the chamber lasted 20.75 hours. Starting at the fifth cycle of exposure, one specimen was tested for lap-shear strength after each cycle. Figure 3 shows that strength decreased linearly with each cycle of exposure up to 12 cycles. From that point on, strengths became very erratic, and many specimens could be broken by routine handling. A compound identified as $Mg(OH)_2$ was deposited in the crevice between the AZ31 and the steel. The deposits were observed after even one exposure, but they continued to thicken with each exposure cycle contributing to a separation force between the sheet specimens. Examination of fracture surfaces found that welded areas also decreased with exposure cycle, but even in the weakest joints there was evidence of metal-metal bonding.

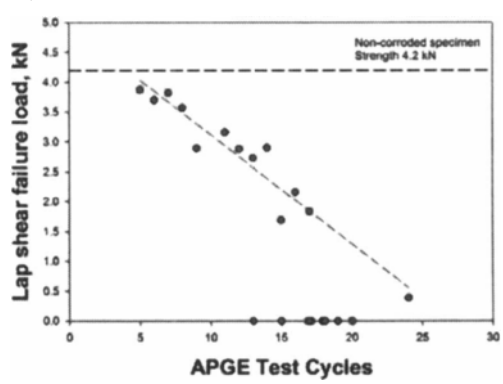

Figure 12. Variations of lap-shear strength and exposure times

Conclusions

A comparative study has been conducted to evaluate the joining potential of Mg/steel couples through two solid state welding routes, e.g., friction stir welding and ultrasonic welding. Initial results in terms of both static and dynamic strengths are very promising. The observed lap-shear strength is higher for FSW route as the bonded area is larger than USW. However, FSW suffers from a restricted configuration of using only Mg as top sheet material. This is not the case for USW method.

The authors would like to acknowledge the support from Dr. Carol Schutte and Mr. William Joost at the US Dept. of Energy, Vehicle Technology, Light Weight Materials Program for this work. This manuscript has been authored by Battelle Memorial Institute, Pacific Northwest Division, under Contract No. DE-AC05-76RL01830 with the U.S. Department of Energy. The United States Government retains and the publisher, by accepting the article for publication, acknowledges that the United States Government retains a non-exclusive, paid-up, irrevocable, world-wide license to publish or reproduce the published form of this manuscript, or allow others to do so, for United States Government purposes.

References

1. www.eere.energy.gov, Vehicle technologies program factsheet, Dec 2010.
2. R.S. Beals, C. Tissington, X. Zhang, K. Kainer, J. Petrillo, M. Verbrugge and M. Pekguleryuz, "Magnesium Global Development: Outcomes from the TMS 2007 Annual Meeting", *JOM*, August 2007, pp. 39-42.
3. S. Jana, Y. Hovanski, G. J. Grant, and K. Mattlin, "Effect of Tool Feature on the Joint Strength of Dissimilar Friction Stir Lap Welds", *Friction Stir Welding and Processing VI*, TMS 2011, pp. 205-211.
4. L.M. Liu, X. Zhao, "Study on the Weld Joint of Mg Alloy and Steel by Laser-GTA Hybrid Welding", *Material Characterization*, 2008, 59, pp. 1279-84.
5. T. Watanabe, K. Kagiya, A. Yanagisawa, and H. Tanabe, "Solid state welding of steel and magnesium alloy using a rotating pin – solid state welding of dissimilar metals using a rotating pin", *Quart J Japan welding soc.*, 2006, 24, pp. 108-15.
6. Y.C. Chen, K. Nakata, "Effect of tool geometry on microstructure and mechanical properties of friction stir lap welded magnesium alloy and steel", *Mat. design*, 2009, 30, pp. 3913-19.
7. W.M. Thomas, E.D. Nicholas, J.C. Needham, M.G. Murch, P. Templesmith, C.J. Dawes, *GB Patent application no. 9125978.8*, December 1991.
8. S. Jana, Y. Hovanski, and G. J. Grant, "Friction Stir Lap Welding of Magnesium Alloy to Steel: A Preliminary Investigation", *Metallurgical and Mat. Trans. A*, 2010, pp. 3173-3182.
9. Klain, P., Knight, D. L., and Thorne, J. P., "Spot Welding of Magnesium with Three-Phase Low Frequency Equipment," *Welding Journal* 32:7-18, 1953
10. Lang: B., Sun, D. Q., Li, G. Z., and Qin, X. F., "Effects of welding parameters on micro-structure and mechanical properties of resistance spot welded magnesium alloy joints *Science and Technology of Welding and Joining* 13:698-704, 2008
11. Teresa J. Franklin, Jwo Pan, Michael Santella, and Tsung-Yu Pan, "Fatigue Behavior of Dissimilar Ultrasonic Spot Welds in Lap Shear Specimens of Magnesium and Steel Sheets," SAE Paper No. 2011-01-0475.
12. Santella, M., T. Franklin, J. Pan, T. Pan, and E. Brown. 2010. Ultrasonic Spot Welding of AZ31B to Galvanized Mild Steel. SAE Paper 2010-01-0975.